Frontiers | Frontiers in Marine Science

TYPE Original Research
PUBLISHED 02 June 2025
DOI 10.3389/fmars.2025.1552576

OPEN ACCESS

EDITED BY
Johan Schijf,
University of Maryland, College Park,
United States

REVIEWED BY
Luigi Jovane,
University of São Paulo, Brazil
José F. García-Hidalgo,
University of Alcalá, Spain
John Rivers,
Queen's University, Canada
Franciszek Hasiuk,
Sandia National Laboratories (DOE),
United States

*CORRESPONDENCE
Hanting Zhong
zhonghanting@cdut.edu.cn
Xia Wang
xiawang@cdut.edu.cn

RECEIVED 28 December 2024
ACCEPTED 14 May 2025
PUBLISHED 02 June 2025

CITATION
Chen C, Zhong H, Wang X, Ning M, Wang X, Wang H, Tang R and Hou M (2025) Recent marine carbonate hardgrounds at Abu Dhabi: towards a better understanding of 'hidden hardgrounds' in the geological past.
Front. Mar. Sci. 12:1552576.
doi: 10.3389/fmars.2025.1552576

Recent marine carbonate hardgrounds at Abu Dhabi: towards a better understanding of 'hidden hardgrounds' in the geological past

Chao Chen[1,2], Hanting Zhong[1,2*], Xia Wang[1,2,3*], Meng Ning[1,2], Xinyu Wang[4], Han Wang[1,2], Ruifeng Tang[5] and Mingcai Hou[1,2]

[1]State Key Laboratory of Oil and Gas Reservoir Geology and Exploitation, Chengdu University of Technology, Chengdu, China, [2]Key Laboratory of Deep-Time Geography & Environment Reconstruction and Applications of Ministry of Natural Resources & Institute of Sedimentary Geology, Chengdu University of Technology, Chengdu, China, [3]Key Laboratory of Sedimentary Basin and Oil and Gas Resources, Ministry of Natural Resources, Chengdu, China, [4]College of Earth and Planetary Sciences, Chengdu University of Technology, Chengdu, China, [5]Exploration Division of PetroChina Southwest Oil & Gasfield Company, Chengdu, China

Marine hardgrounds are common features during the Phanerozoic and hold significant sedimentological and economic importance. Intriguingly, previous reports of marine hardgrounds are concentrated in Calcite Seas, despite elevated seawater $CaCO_3$ saturation in Aragonite Seas. This bias remains unclear in origin and requires more hardground information, especially from Aragonite Seas, for clarification. Well-developed Holocene marine hardgrounds at Abu Dhabi provide such a good opportunity. This study focused on a widespread and well-developed Holocene marine hardground layer at Abu Dhabi and analyzed its chronostratigraphy, petrology, mineralogy, and geochemistry. The results show that the studied hardground layer can be divided into lower and upper parts, characterized by planar upper surface and no borings nor encrustations. The lower part (with a ^{14}C age of 6945–6368 cal yrs BP) formed during a sea-level transgression, and is laterally traceable along both a seaward and a landward direction. The upper part (with a ^{14}C age of 5871–5452 cal yrs BP) formed during following sea-level transgression and/or stillstand, and disappears along a landward direction. Compared with the lower part, the upper hardground part is higher in $\delta^{13}C_{carb}$ and $\delta^{18}O_{carb}$, supporting formation within more evaporated seawater settings depositing more high-Mg calcite. Both parts consist mainly of aragonite and high-Mg calcite in both carbonate grains and intergranular early-marine cement, but the lower hardground part contains more protodolomite within the early-marine cement. Moreover, an inverse relation in contents indicates a diagenetic transition from aragonite to dolomite during hardground formation and early diagenesis. Further, in combination with previous studies, the findings of this study confirm the rapidity, lateral diachronicity, and composite nature of Holocene marine hardgrounds with mineralogy controlled by sea-level changes. Similar hardgrounds may also be well developed in ancient records (especially in Aragonite Seas like the modern ocean), but be ignored due to lack of recognizable features (e.g., boring, irregular upper surfaces, Fe-Mn encrustation) and mineral recrystallization. These "hidden hardgrounds" and their composite formation by diachronous parts have implications for sequence stratigraphy and hydrocarbon exploration using hardgrounds in stratigraphic correlation.

KEYWORDS

Arabian/Persian Gulf, holocene, hardgrounds, carbonate cement, early-marine diagenesis

1 Introduction

Marine hardgrounds occurred widely in ancient strata, dating back to the Precambrian at the earliest, but are more common during the Phanerozoic (Christ et al., 2015). Hardgrounds are features in the sediment record that present evidence for significant early marine cementation of the seafloor itself and/or portions of the near-seafloor sediment column (Christ et al., 2015). It is generally believed that cementation occurs in the marine phreatic early diagenetic environment (Shinn, 1969; Paul and Lokier, 2017; Millo et al., 2022). They are often used as marker layers for stratigraphic correlation (Immenhauser et al., 2000; Rais et al., 2007; Yilmaz et al., 2012; Godet et al., 2013; Christ et al., 2015; Brigaud et al., 2021). Moreover, marine hardgrounds can serve as fluid barriers during water and hydrocarbon exploration (Read and Horburry, 1994; Cander, 1995; Wagner et al., 1995; Mancini et al., 2004; Eren, 2022). Marine hardground cements are also a useful tool for looking at past environmental and oceanographic changes but multiple geochemical proxies must be used to tease apart the various constraints (Erhardt et al., 2020).

The conventional view is that marine hardgrounds form at low sedimentation rates and/or during erosional intervals (Shinn, 1969; Mutti and Bernoulli, 2003; Paton et al., 2019; Basilone et al., 2024), hence representing sedimentary hiatus. Marine hardgrounds often form during sea-level transgression (Gruszczyński et al., 2002; Catuneanu, 2006; McLaughlin et al., 2008; Catuneanu et al., 2009) and have irregular morphologies by boring, bio-encrustation, and/or Fe-Mn encrustation (Bathurst, 1975; Moore, 1989; Di Stefano and Mindszenty, 2000; Vinn and Wilson, 2010; Grădinaru et al., 2011; Conti et al., 2013; Wright and Cherns, 2016; Paton et al., 2019; Matysik et al., 2022; Hu et al., 2023).

However, previous studies have also recognized hardgrounds forming during high sedimentation rates at the Bahamas (Dravis, 1979). Due to the lateral variability of hardgrounds, the utilization of marine hardgrounds for stratigraphic correlation may also cause misinterpretation (Sattler et al., 2005). The chemical composition of Phanerozoic seawater oscillated between Calcite Seas (the dominance of low-Mg calcite in abiotic marine $CaCO_3$ precipitates, in which the Mg/Ca ratios are < ~2, and slow rates of sea-floor spreading are present) and Aragonite Seas (the dominance of aragonite and high-Mg calcite in abiotic marine $CaCO_3$ precipitates, in which the Mg/Ca ratios are > ~2, and fast rates of sea-floor spreading are present). Interestingly, the secular distribution of ancient marine hardgrounds shows a bias towards Calcite Seas in previous studies (see review in Christ et al., 2015). This bias is strange given higher seawater $CaCO_3$ saturation during Aragonite Seas which is more favorable for early marine cementation and hardground formation. The temporal distribution of ancient marine hardgrounds may indicate the existence of unrecognized ("hidden") hardgrounds formed in Aragonite Seas, which have different features relative to that in Calcite Seas. Alternatively, the fewer reports of marine hardgrounds in Aragonite Seas may be related to preservation, as aragonite is easily altered during diagenesis (Christ et al., 2015). To reveal the potential of "hidden" hardgrounds, an in-depth understanding of marine hardground formation in the Aragonite Sea is necessary.

Given the problems above, widespread and well-developed Holocene marine hardgrounds in the Abu Dhabi coastal area were investigated (Shinn, 1969; Paul and Lokier, 2017; Ge et al., 2020). This study focused on timing, mineralogical features, and formation processes of these hardgrounds, and aimed to provide new insights into ancient "hidden" hardgrounds and the application of hardgrounds in stratigraphic correlation and hydrocarbon exploration.

2 Geological setting

The study area is located in the Abu Dhabi coastal area, the southeast part of the Arabian/Persian Gulf (Figure 1A). The area represents a low-angle (0.07~0.08°) carbonate ramp within a modern epeiric sea (Ge et al., 2020; Pederson et al., 2021) (Figure 1A). The present topography of the coastal area is sculpted by sea-level fluctuations related to glaciation. The Last Glacial Maximum (26.5 to 19 kyrs BP) led to a regional sea-level fall with sea level of ca 120 to 130 m lower than the present-day level (Fleming et al., 1998; Clark et al., 2009; Hanebuth et al., 2009). During the lowstand period, the sea floor of the Persian Gulf was exposed and dominated by terrestrial aeolian deposits (Lokier et al., 2015). After the termination of the Glacial Maximum, a Holocene transgression from 7100 to 5290 cal yrs BP led to hardground formation and shallow subtidal deposition in the coastal area (Lokier et al., 2015; Paul and Lokier, 2017; Figure 1B). Then the

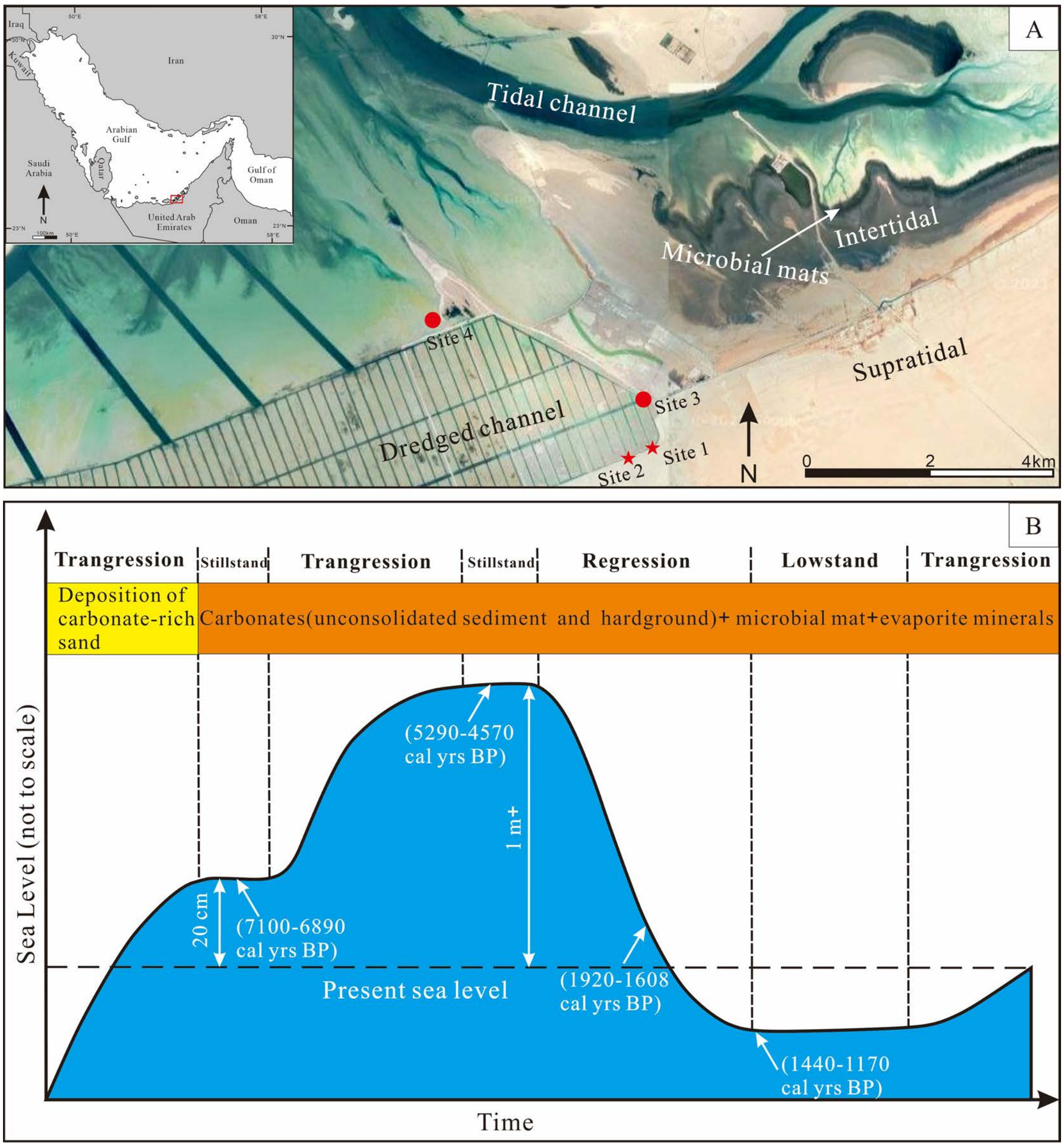

FIGURE 1
Sampling location and sea level history in the study area. **(A)** The study area is located in the southwestern part of the Arabian/Persian Gulf (red rectangle in the insert of **(A)**). Sampling sites in this study are sites 1 & 2 (indicated by red star), while sampling sites (site 3 & 4 indicated by red circle) are from Paul and Lokier (2017). **(B)** Relative regional sea-level history in the Abu Dhabi region and associated sedimentation. Modified from Lokier et al. (2015) and Paul and Lokier (2017).

Abu Dhabi region experienced a regression until about 1440–1170 cal yrs BP, which led to the precipitation of evaporite minerals in the shallow sub-surface (Lokier et al., 2015). Finally, this area experienced a transgression to the present (Lokier et al., 2015). Therefore, below the surface of the present-day middle and upper intertidal zones and in the supratidal zones, marine hardground is covered by a succession of carbonate, evaporite, and microbial sediments with increasing thickness (Lokier and Steuber, 2008).

The Abu Dhabi coastal area has a hot and dry climate, and an average annual rainfall of only 72 mm, 74% of which is concentrated in February and March (Lokier, 2013). The Abu Dhabi area experiences temperatures ranging from 7°C to over 50°C, with daily temperature differences between 2°C and 26°C (Lokier, 2013; Lokier and Fiorini, 2016; Paul and Lokier, 2017). The prevalent wind pattern is the northwest-blowing Shamal.

Recent marine carbonates massively accumulate in the Abu Dhabi coastal areas with both loose carbonate grains and well-developed and widespread hardgrounds (Shinn, 1969; Paul and Lokier, 2017; Ge et al., 2020). Modern hardgrounds exposed on the present seafloor are cemented by various aragonite and high-Mg calcites and show lateral variability in morphological features and formation processes (Ge et al., 2020). On the other hand, Holocene marine hardgrounds have been exposed in the dredged channels on the sabkha and have been suggested to be related to sea-level fluctuations in terms of formation processes and can help shoreline stabilization (Paul and Lokier, 2017).

3 Materials and methods

3.1 Field sampling

Holocene marine hardgrounds were sampled along the dredged channels for analyses (Figure 1A). This includes a landward site (Site 1, N 24°6'47.74", E 54°3'25.79"; Figures 2A-C) and a seaward site (Site 2, N 24°6'46.64", E 54°3'23.99"; Figures 2D, E). The mid to late Holocene succession in this area shows the following profile from base to top: (1) carbonate-rich sand; (2) Holocene marine hardground; (3) skeletal-peloid packstone/grainstone; (4) gypsum-rich bioclastic grainstone.

3.2 Optical and scanning electron microscope analyses

Thin sections were made from collected hardground samples to investigate sedimentary components and cements. The thin sections were dyed with Alizarin red to distinguish between dolomite and calcite (Friedman, 1959). Photographs were taken using a Nikon optical microscope (Nikon LV100POL).

Small pieces of freshly broken hardground samples were selected and coated with Platinum. Then, a Hitachi S-4800 scanning electron microscope (SEM) coupled with electron-dispersive spectroscopy (EDS) at Chengdu Geological Survey Center (China Geological Survey) was used to observe the carbonate microfabrics minerals, and chemical compositions in the hardgrounds.

3.3 X-ray diffraction analyses

Powder samples from the hardgrounds were prepared using a handheld drill for XRD analyses. Along the bottom-to-top direction in the hardgrounds, the powder samples were taken with an interval of approximately every 1 cm. The XRD measurement was performed at Shiyanjia Lab using Rigaku D/MAX-2600. The measuring range was between 5 and 90° 2θ.

3.4 Radiocarbon dating

The hardground samples were dated based on Accelerator Mass Spectroscopy (AMS) ^{14}C radiocarbon dating (State Key Laboratory of Organic Geochemistry, Guangzhou Institute of Geochemistry, Chinese Academy of Sciences). Gastropod grains from the seaward hardground were obtained at positions of 0.5 cm, 5.0 cm, 6.0 cm, and 7.5 cm above the hardground bottom respectively. In addition, gastropod grains were also extracted from the bottom of the landward hardground. Secondary cements were removed and a pretreatment procedure based on acid etch was performed before AMS measurement. The measured values were calibrated in OxCal v4.4.4 Bronk Ramsey with the Marine20 calibration curve (Heaton et al., 2020). In addition, a regional reservoir age correction (ΔR) of 180 ± 53 years was applied, as derived from a sample collected off the coast of the Qatar peninsula (Hughen et al., 2004; Paul and Lokier, 2017). The results of radiocarbon ages are reported in calibrated years before the present (cal yrs BP).

3.5 Geochemical analyses

The $\delta^{18}O_{carb}$ and $\delta^{13}C_{carb}$ analyses of the bulk carbonates were made at Nanjing Hongchuang Geological Technology Co. Ltd. About 100 μg sample powder was weighed, and the powders were placed in a CTC Combi-Pal and reacted with H_3PO_4 at 72°C, with reacting time of 4h for calcite and 24h for dolomite to produce CO_2. Subsequently, the CO_2 was analyzed with the MAT253 gas stable isotope mass spectrometer (Thermo Fisher Scientific, USA). In order to ensure accuracy, the standard GBW04405 ($\delta^{13}C_{VPDB}$ = 0.57‰; $\delta^{13}C_{VPDB}$ = −8.49‰) was processed and analyzed simultaneously with the samples, and the analytical precision is better than 0.1‰. The results were reported relative to the Vienna PeeDee Belemnite (V-PDB) scale.

4 Results

4.1 Petrological characteristics of hardgrounds

The marine hardground layer contains one subsection in site 1 (Figure 2C), while contains two subsections separated by a clear boundary in site 2 (Figure 2E). At both sites, the hardgrounds are underlain by unconsolidated aeolian siliciclastic sands and are overlain by modern sabkha sediments including loose carbonates, gypsum deposits and halite crusts (Figure 2A). At both sites, marine hardgrounds have planar top surfaces with no borings and irregular lower surfaces (Figures 2C, E).

In site 1, the hardground layer is 3 cm to 4 cm thick and consists mainly of bioclasts with peloids and quartz grains (Figure 2C). The bioclasts include benthic foraminifera, bivalves, gastropods, and ostracods (Figure 3A). Fibrous aragonite cements occupy the inter-grain pore space (Figure 3B).

In site 2, the lower hardground part layer varies in thickness between 3 and 5 cm. It consists mainly of bioclasts (gastropods, bivalves, benthic foraminifera) and peloids (Figures 3C-F). Micritic rims occur around large bioclasts (Figures 3E, F). Moreover, the non-carbonate grains are dominated by aeolian siliciclastic quartz, which is fine- to very fine-grained and sub-rounded to angular (Figure 3D). Both intergranular and intragranular pores are observed (Figures 3C-E).

The upper hardground part in site 2 has a thickness of about 3 cm and also consists mainly of bioclasts. The carbonate grain types are similar to those in the lower part, but the quartz content decreases. Fibrous aragonite cements locally occupy the intergranular pores (Figures 3G-I).

4.2 Mineralogical composition of the hardgrounds

4.2.1 Bulk mineralogical variation

Based on the XRD analysis, carbonate minerals in the hardgrounds include aragonite, high-Mg calcite, calcite, and protodolomite (Table 1; Figure 4).

In the hardground in site 1, the aragonite content increases from 69.5% at the base to 81.5% at the top of the hardground. In contrast, high-Mg calcite and protodolomite contents decrease from 19.3% and 4.7% to 12.0% and 1.1%, respectively, from the bottom to the top of the hardground.

In the lower hardground part in site 2, the aragonite content increases from 63.9% at the base to 72.9% at the boundary

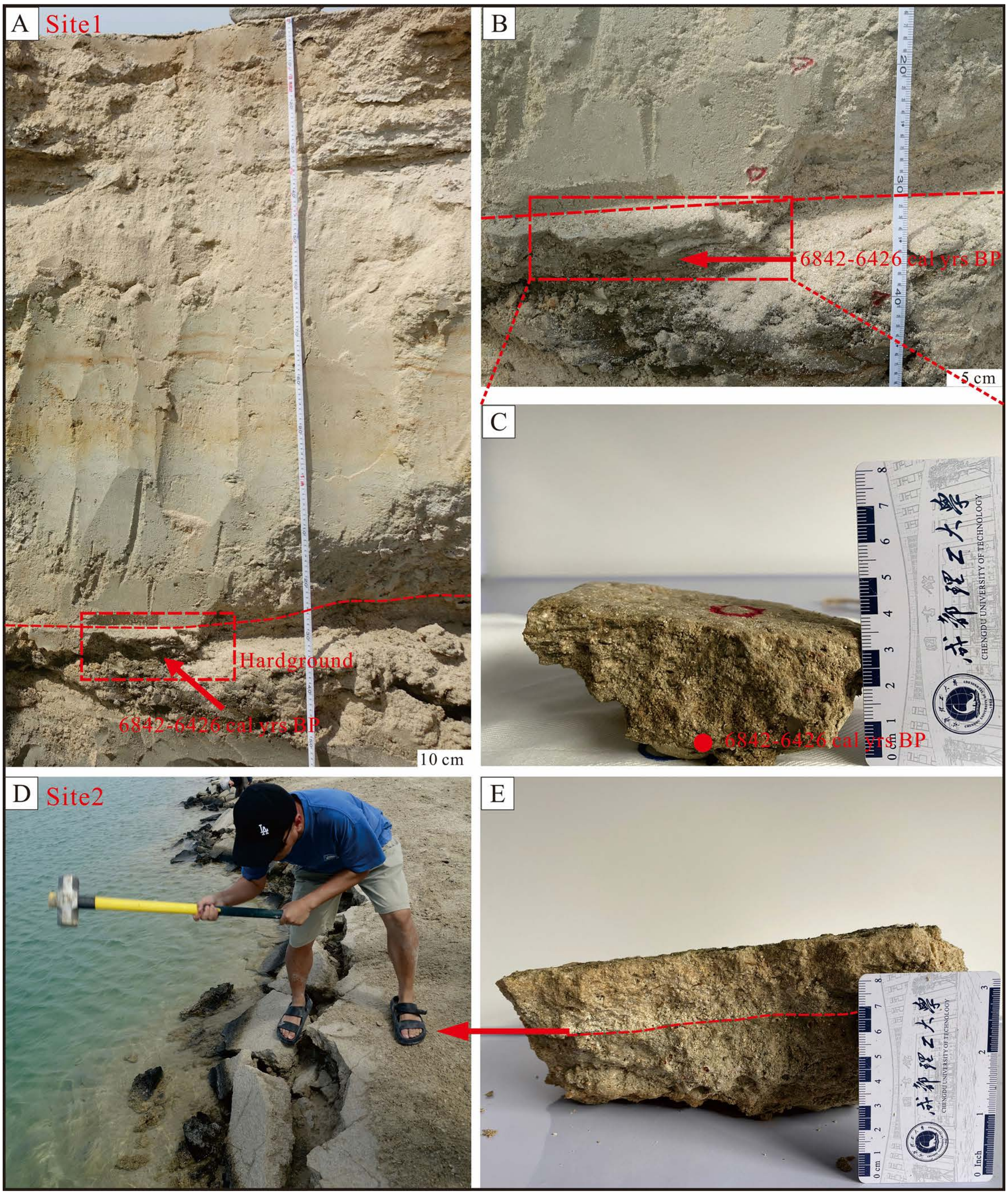

FIGURE 2
Holocene marine hardgrounds in the sampling sites. **(A)** The hardground in site 1 (indicated by the red frame), is covered by loose carbonate and evaporite sediments. **(B)** Close-up of the specific location of the hardground **(A)** in the outcrop. ^{14}C ages of the hardgrounds and overlying loose carbonates are labelled. **(C)** A further close-up view of the hardground at site 1 with a ^{14}C age of 6842–6426 cal yrs BP at the bottom. **(D)** Holocene marine hardgrounds exposed in a dredged channel at site 2. **(E)** Close-up view of the hardground at site 2, showing a boundary between the lower and the upper parts.

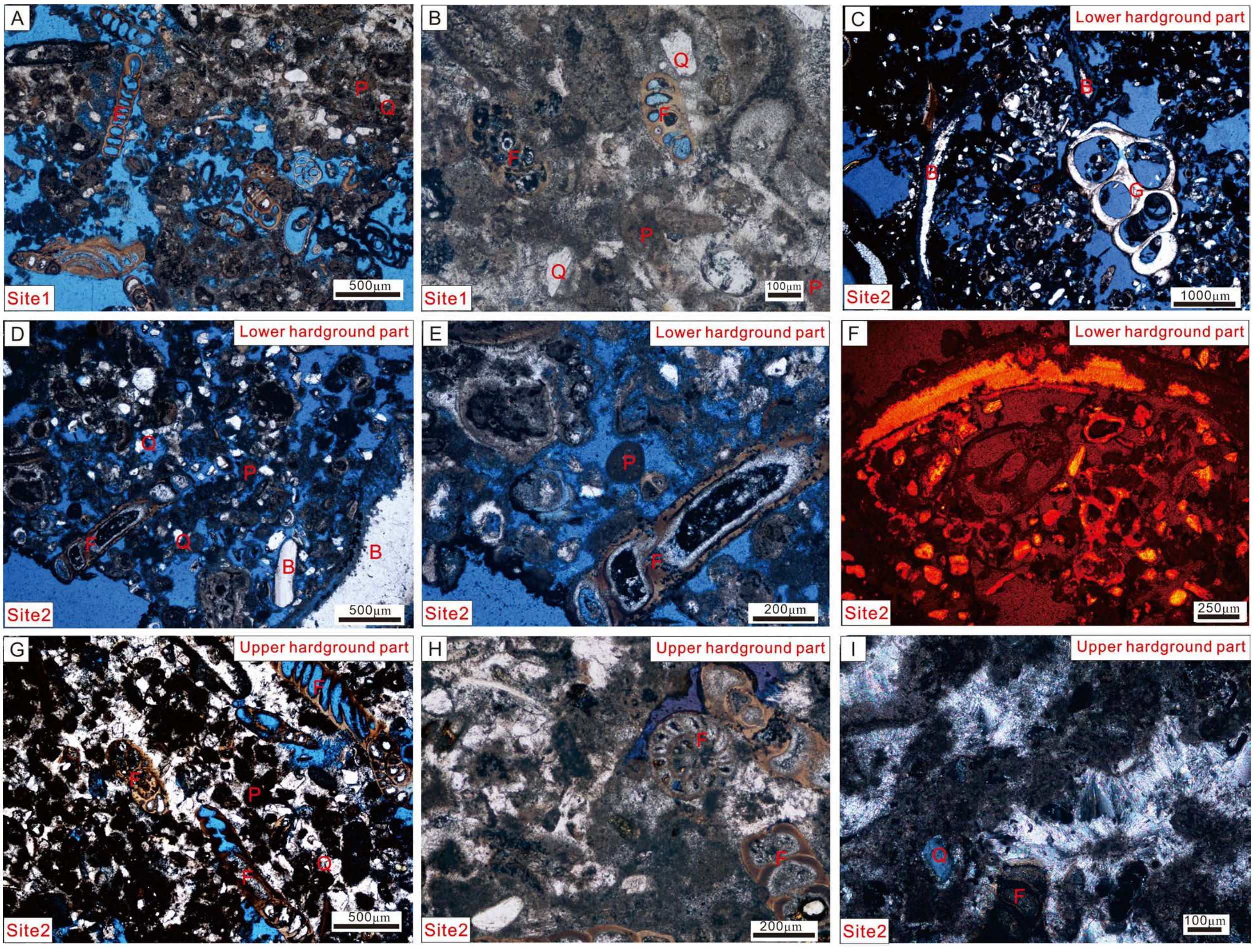

FIGURE 3
Sedimentary features of the hardgrounds in thin sections. **(A)** The hardground at site 1 contains benthic foraminifera and peloids. The intergranular pores and intragranular pores are observed. **(B)** In the hardground at site 1, the light color between benthic foraminifera and peloids is fibrous aragonite cement. **(C)** The lower hardground part in site 2 contains gastropod and bivalve shells. **(D)** The lower hardground part in site 2 shows peloids, benthic foraminifera, and bivalve shells. **(E)** The lower hardground part in site 2 with peloids and benthic foraminifera. **(F)** The lower hardground part in site 2 under cathodoluminescence. Micrite envelopes are visible at the edge of the shell. **(G)** The upper hardground part in site 2 contains benthic foraminifera, peloids, and quartz grains. The light color between the grains is aragonite or high-Mg calcite cement. **(H)** The upper hardground part in site 2 with peloids and benthic foraminifera. The intergranular pores are filled with fibrous aragonite cement. **(I)** The upper hardground part in site 2 under cross-polarized light. The primary pore space between peloidal and bioclastic grains is filled with fibrous aragonite cement. Q, quartz; P, peloid; B, bivalve; G, gastropod; F, benthic foraminifer.

TABLE 1 Carbonate mineralogical compositions in the hardground based on XRD analysis.

Location	Sample	Aragonite	High-Mg calcite	Low-Mg calcite	Protodolomite
Site 1	ADP4-1-T	81.5	12.0	5.4	1.1
	ADP4-1-B	69.5	19.3	6.6	4.7
Site 2	ADP5-1	57.4	30.8	7.4	4.5
	ADP5-2	62.5	28.3	6.7	2.5
	ADP5-3	70.7	19.2	7.4	2.6
	ADP5-4	72.9	9.9	11.2	6.0
	ADP5-5	70.1	11.9	6.9	11.1
	ADP5-6	63.9	13.7	8.2	14.3

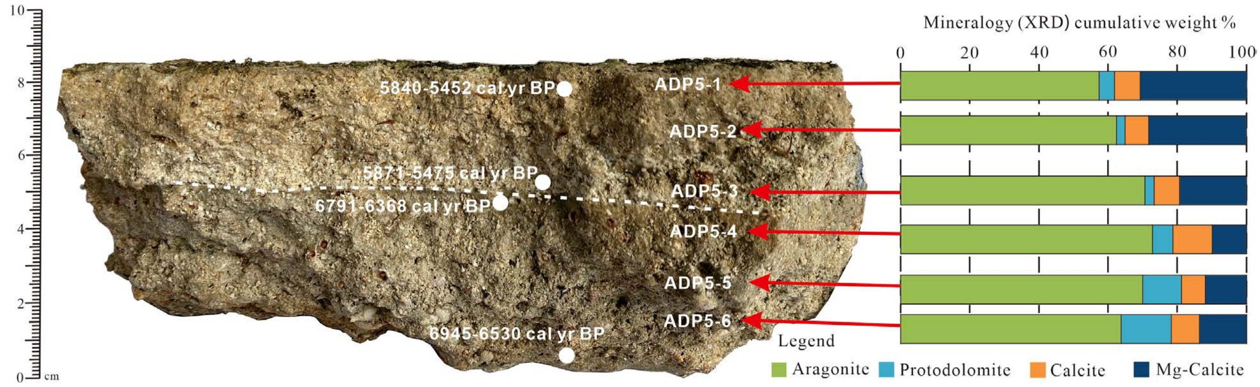

FIGURE 4
Radiocarbon dating and carbonate mineralogical compositions of the marine hardground in site 2.

separating the lower and upper part, and high-Mg calcite and protodolomite contents decrease from 13.7% and 14.3% to 9.9% and 6.0%, respectively, from the bottom to the boundary. Meanwhile, the calcite content does not show a clear trend.

In the upper hardground part in site 2, the aragonite content decreases from 71% at the internal boundary to 57% at the top, and the high-Mg calcite and protodolomite contents increase from 19% and 2.6% to 31% and 4.5%, respectively, from the boundary to the top.

4.2.2 Cement mineralogy

Overall, the marine hardgrounds are cemented by aragonite, high-Mg calcite, and protodolomite (Figure 5). The presence of poorly-ordered protodolomite was confirmed by the XRD identification (Figure 6) and observations with SEM-EDS (Figure 5I). In the lower hardground part at site 2, fibrous aragonitic cements are oriented perpendicular to grain surfaces and occur as isopachous fringes around bioclasts and peloids (Figure 5A). Meanwhile, prismatic aragonite, micritic high-Mg calcite, and protodolomite are also observed in the lower part of the hardground (Figures 5B, C).

In the upper hardground part at site 2, the morphology of aragonitic cements mainly includes acicular, fibrous, and elongated prismatic (Figures 5D, E). The orientation of the acicular and fibrous aragonitic cements is perpendicular to carbonate grain surfaces (Figure 5D). Microbial filaments were found among fibrous aragonites (Figure 5D). Some prismatic aragonite cements have voids at the crystal terminations (Figure 5E). In addition, the micritic high-Mg calcite shows small platy sub-crystals and irregular surfaces (Figure 5F), while platy and fibrous high-Mg calcites are also observed (Figures 5G, H). The protodolomite cement is mainly rhombohedral in shape (Figure 5I). High-Mg calcite and protodolomite cements either coat grain surfaces as thin rims or accumulate as micro-peloids (Figures 5G-I).

In the hardground at site 1, the cement mineralogy includes fibrous, prismatic aragonites and platy, rhombohedral high-Mg calcites. Their morphology is similar to the cement of the hardground in site 2.

4.3 Radiocarbon age of the hardgrounds

In the hardground in site 1, the radiocarbon age of the gastropods from the hardground base was 6842–6426 cal yrs BP (Figure 2A). The hardground is covered by approximately 1.3 m of sediment and is capped by the present-day modern sabkha sediments (Figure 2A).

At site 2, in the lower hardground part, the radiocarbon ages of the gastropods from the base and the top of the hardground were 6945–6540 cal yrs BP and 6791–6368 cal yrs BP respectively (Figure 4). In the upper hardground part in site 2, the ^{14}C ages of the gastropods from near the base and the top were 5871–5475 cal yrs BP and 5840–5452 cal yrs BP respectively (Figure 4).

4.4 Geochemical features of the hardgrounds

In the hardground in site 1, the $\delta^{13}C_{carb}$ values are in the range of 3.31 to 3.70‰, with an average value of 3.51‰. The $\delta^{18}O_{carb}$ values vary from 1.03 to 2.15‰, with an average value of 1.59‰. In the lower hardground part in site 2, the $\delta^{13}C_{carb}$ values are in the range of 3.65 to 3.79‰, with an average value of 3.72‰. The $\delta^{18}O_{carb}$ values vary from 0.91 to 1.30‰, with an average value of 1.16‰. In the upper hardground part in site 2, the $\delta^{13}C_{carb}$ values are in the range of 4.04 to 4.28‰, with an average value of 4.18‰. The $\delta^{18}O_{carb}$ values vary from 1.08 to 1.41‰, with an average value of 1.21‰ (Table 2).

5 Discussion

5.1 Typical ancient vs. atypical Holocene hardgrounds: a potential analogue for the "hidden hardgrounds"

Previous studies have documented the formation process of typical marine hardgrounds. Most studies interpreted that the

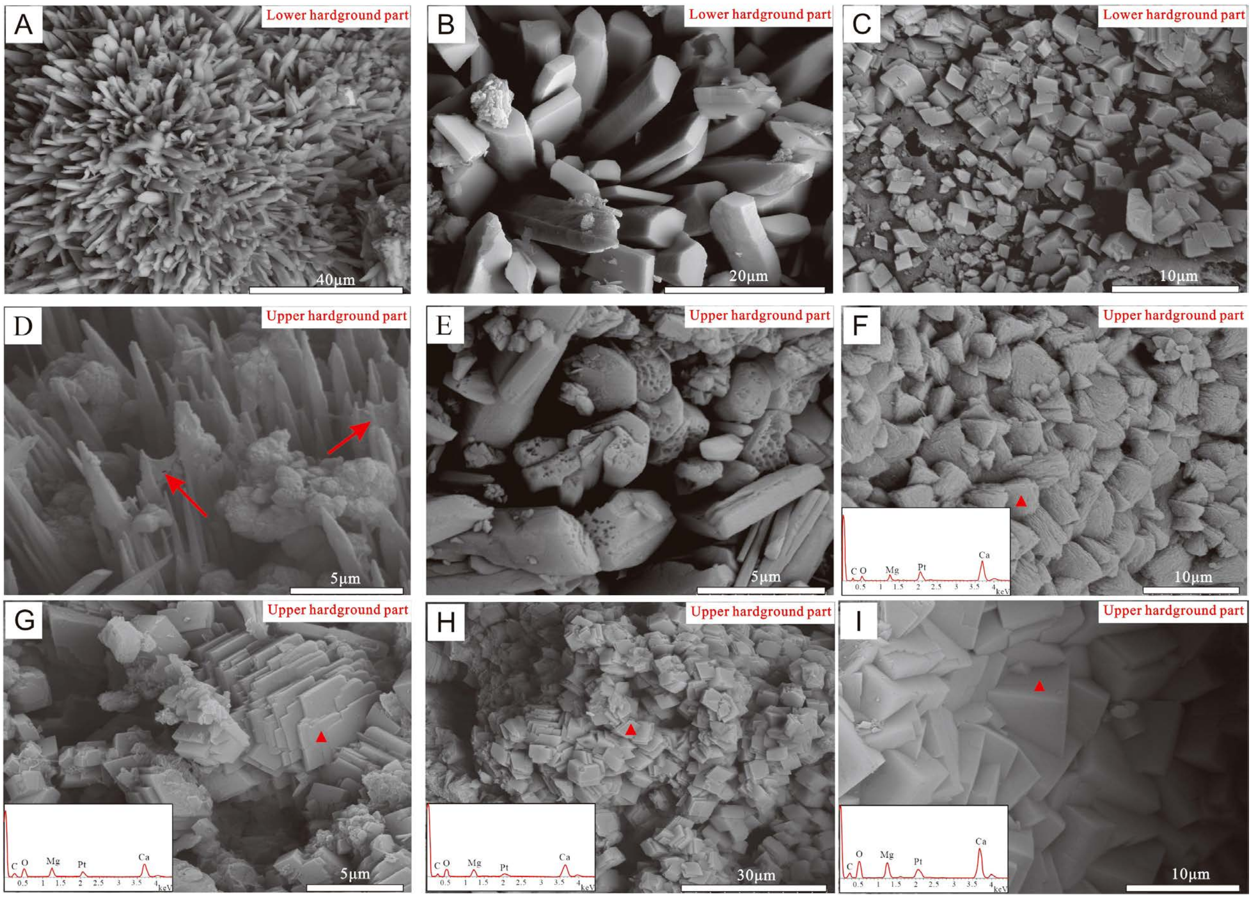

FIGURE 5
Carbonate cement features based on SEM-EDS analysis. **(A–C)** Scanning electron microscope images of the cements of the lower hardground part in site 2. **(A)** Fibrous aragonitic cements are perpendicular to the particle surface. **(B)** Prismatic aragonite cements growing into primary pore space. **(C)** Rhombohedral high-Mg calcites grow randomly on the surface of the particles. **(D-I)** Scanning electron microscope images of the cements of the upper hardground part in site 2. **(D)** Acicular (needle) aragonitic cements, with associated microbial filaments (red arrow). **(E)** Prismatic aragonite cements with voids at the termination. **(F)** Micritic high-Mg calcite cements show irregular surfaces and smaller platy sub-crystals (red triangle refers to EDS data). **(G)** Platy rhombohedral high-Mg calcite crystals are superimposed to form rhombohedral crystals (red triangle refers to EDS data). **(H)** SEM of radiaxial fibrous Mg calcites (red triangle refers to EDS data). **(I)** Rhombohedral protodolomite crystals are superimposed on each other (red triangle refers to EDS data).

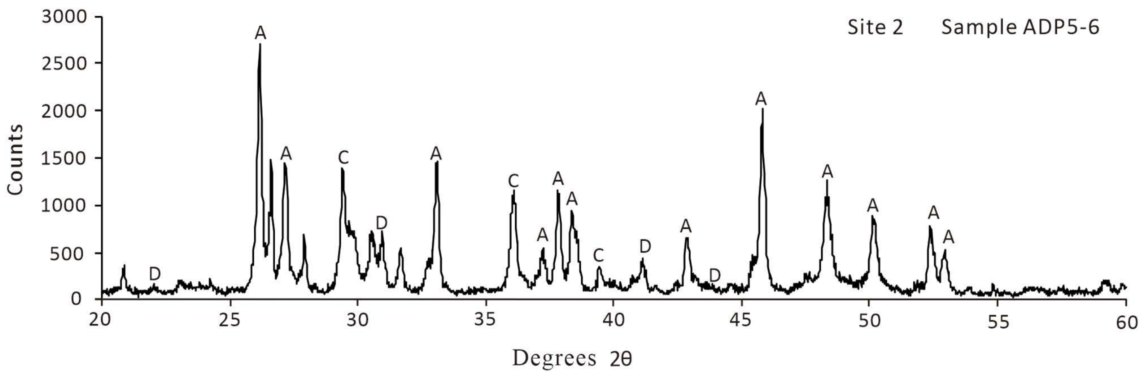

FIGURE 6
X-ray diffraction patterns of the sample ADP5–6 from the lower hardground part of site 2. Dolomite peaks are indicated with 'D'. The peaks 'A' and 'C' refer to aragonite and calcite, respectively.

TABLE 2 Analytical results of$\delta^{13}C_{carb}$ and $\delta^{18}O_{carb}$ in the hardground samples .

Sample name	$\delta^{13}C_{carb}$ ‰	$\delta^{18}O_{carb}$ ‰
ADP4-1-B	3.31	2.15
ADP4-1-T	3.70	1.03
ADP5-1	4.23	1.41
ADP5-2	4.04	1.15
ADP5-3	4.28	1.08
ADP5-4	3.79	1.30
ADP5-5	3.71	1.27
ADP5-6	3.65	0.91

formation of hardground is owing to the lithification of loose carbonate grains by carbonate cements, and the carbonate cements are mainly synsedimentary and inorganic precipitation of carbonates (Wilson and Palmer, 1992; Rozhnov, 2001; Palmer and Wilson, 2004; Lee et al., 2015). Paton et al. (2019) believed that carbonate cementation in marine environment occurred in sulfate reduction zone. An increase of alkalinity and porewater supersaturation with respect to $CaCO_3$ in sulfate reduction zone leads to precipitation of cements, thereby lithifying the carbonate sediments. Due to the time required for lithification of carbonate sediments and subsequent erosional exhumation (Wilson and Palmer, 1992; Paton et al., 2019), the low sedimentation rate and erosion period are conducive to the alkalinity elevated zone to maintain a relatively constant depth below the sediment-water interface. Under prolonged sedimentary hiatus, early cementation resulted in the formation of hardgrounds with a thickness of centimeter to decimeter scale (Kennedy and Garrison, 1975; Christ et al., 2015). Therefore, marine hardgrounds generally represent sedimentary hiatus (Immenhauser et al., 2000; Sattler et al., 2005; Rameil et al., 2012). Typical ancient marine hardgrounds formed at roughly the same time (Mutti and Bernoulli, 2003), are widely distributed in regional area (Gruszczyński et al., 2002), and go through different stages from firm- to hardground (Kennedy and Garrison, 1975; Christ et al., 2015; Pandey et al., 2018). In addition, boring, bio-encrustation and Fe-Mn encrustation are often diagnostic features of typical ancient marine hardgrounds (Warme, 1975; Wignall, 1993; Paton et al., 2019; Matysik et al., 2022).

By contrast, the Holocene marine hardgrounds in this study show obvious differences and are characterized by flat upper surface with few borings and/or encrustation, rapid cementation with active carbonate deposition, composite formation, and diachroneity. These unconventional features may represent those of the hidden hardgrounds during the geological past that may be ignored and less investigated in previous studies. These features of the Holocene marine hardgrounds are discussed in detail in the following sections.

5.2 Rapid formation with a short duration

Duration refers to the timescale over which diagenetic and lithification processes occur. Here, it refers to the time required for hardground formation. In ancient records, marine hardgrounds often represent sedimentary hiatus with a long duration with a low sedimentation rate (Sattler et al., 2005; Rameil et al., 2012; Christ et al., 2015; Paton et al., 2019). By contrast, the widespread Holocene hardground layer in the modern Abu Dhabi area presents much faster formation rates (a few hundred years) with active carbonate deposition (rather than sedimentary hiatus). Based on ^{14}C dating, the formation of the lower hardground part in site 2 may correspond to 200 to 600 cal yrs BP, while the formation of the upper hardground part in site 2 may correspond to 30 to 400 cal yrs BP. The rapid hardground formation can also be evidenced by containing abundant aragonitic carbonate grains and cements components that are easily recrystallized in burial diagenesis (Figure 4).

In line with this study, previous studies from modern shallow, tropical-subtropical marine environments also suggest a fast rate of hardground formation (Table 3). Weakly (Figure 7A) to fully lithified hardgrounds (Figure 7B) are both observed in the modern intertidal zone of Abu Dhabi. The ^{14}C ages of these modern marine hardgrounds, ranging from 268 to 0 cal yrs BP (Ge et al., 2020), support that the hardground formation is very quick following modern sediment deposition. Further, the modern marine hardgrounds exhibit all stages of lithification, from weak to strong early cementation in recent carbonate sediment (see Figure 8 in Ge et al., 2020), implying very fast cementation rates. In the

TABLE 3 Cementation rates of modern-Holocene marine hardgrounds.

Era/geographic location	Bathymetric setting	Time involved in seafloor lithification/Dating method	Reference
Holocene/Arabian Gulf	Neritic	<20 years/observations	Shinn, 1969
Holocene/Arabian Gulf	Neritic	<4500 years/^{14}C	Taylor and Illing, 1969
Recent/Bahamas	Neritic	Several months/observations	Dravis, 1979
Recent/Jamaica	Neritic	<130–140 years/^{14}C	Pigott and Land, 1986
Recent/Bahamas	Neritic	<1 year/observations	Friedman, 1998
Recent/Bahamas	Deeper platform	<1 year	Grammer et al., 1999
Holocene/Arabian Gulf	Neritic	<900 years/^{14}C	This study

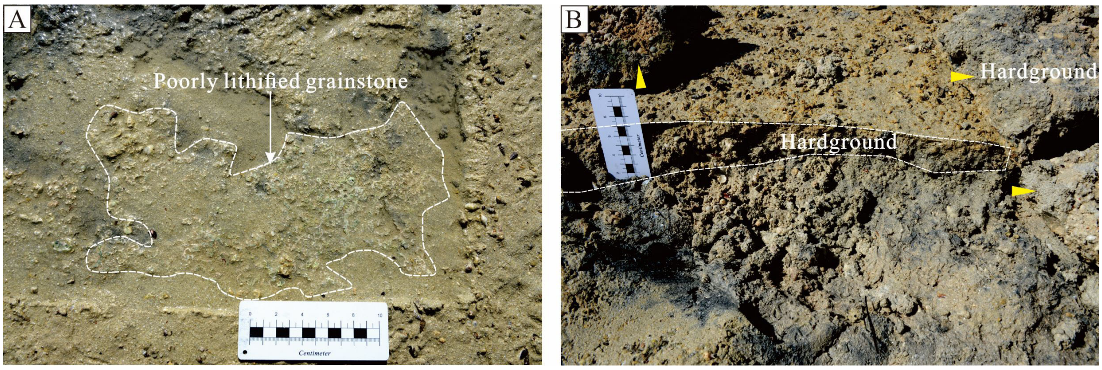

FIGURE 7
Early marine lithification with different cementation degrees. **(A)** Poorly lithified carbonate sediments (indicated by white frame) covered by about 1 cm thick loose carbonates in the intertidal zone of Abu Dhabi. **(B)** Better lithified carbonate sediments (indicated by yellow triangles) that are a few meters away from **(A)**, with a flat top surface and irregular lower surface.

Arabian/Persian Gulf, Shinn (1969) also noted that, in shallow subtidal environments, the process of sediment lithification was almost synsedimentary. Dravis (1979) observed that oolitic crusts in the Bahamas may form in a few months or even less. Friedman (1998) reported shallow water carbonate sediments were cemented within a year during periods of high sea level. Marine cementation in the carbonate platform margin environments can also occur in a few months (Grammer et al., 1999). The compilations above clearly show that marine hardground formation can happen quickly (<1 kyr) in an Aragonite Sea, with active carbonate deposition.

A recent study by Pederson et al. (2021) demonstrates that contemporary coastal seawater in Abu Dhabi exhibits aragonite supersaturation. Notably, symmetrical wave ripples, which are characteristic sedimentary structures of modern intertidal environments (Lokier et al., 2013; Ge et al., 2020), have been documented within the upper part of the hardground at site 3 (Paul and Lokier, 2017). This evidence supports that the hardground formation in this study is due to rapid cementation related to the pumping of supersaturated seawater thought the sediment by tides and waves. Similar mechanisms have also been

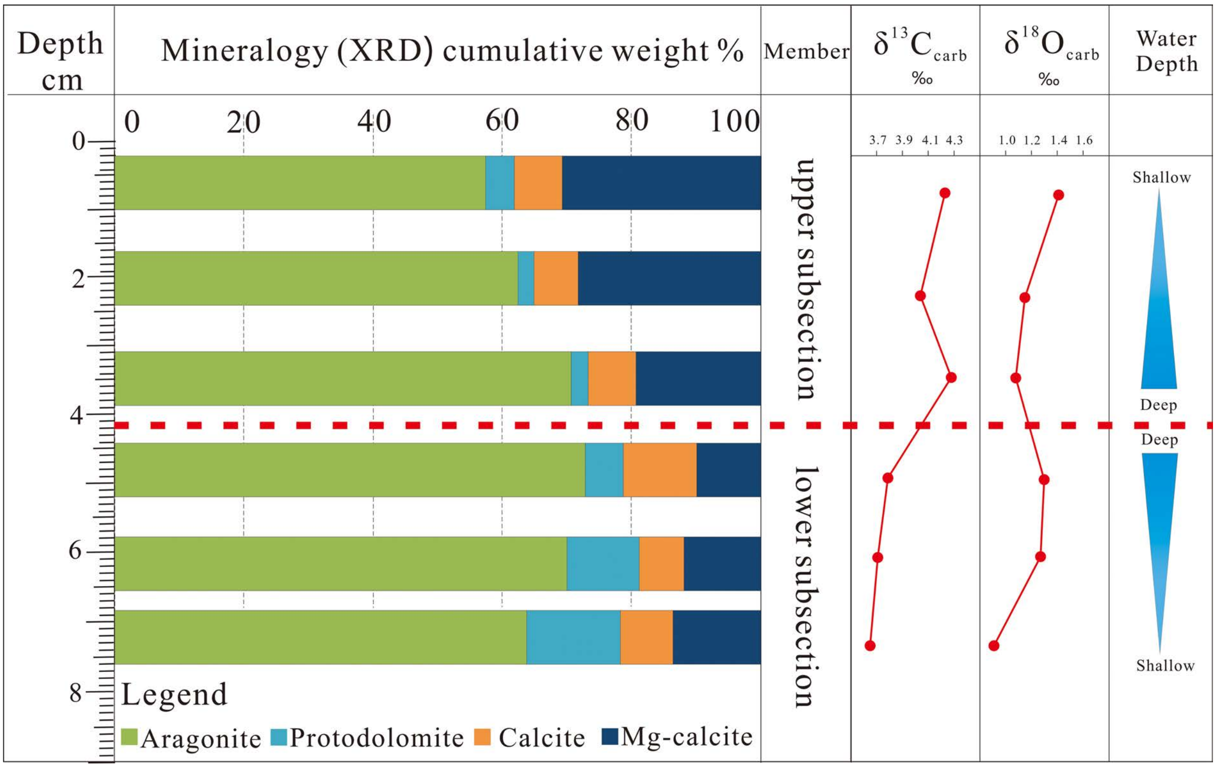

FIGURE 8
Mineralogical and isotopic features of the hardground layer in site 2.

reported in other studies (Dravis, 1979; Tucker and Wright, 1990; Schlager et al., 1994).

The lack of borings, erosion, and encrustations in these hardgrounds may be due to the short time of exposure to the seafloor (Brett and Brookfield, 1984), protection by overlying sediment (Shinn, 1969), and/or seawater properties (e.g., high salinity) (Ge et al., 2020).

5.3 Composite nature of the hardground formation and its relationship with sea-level changes

As shown by the petrological and ^{14}C dating features, the hardground layer at site 2 consists of two parts. The lower hardground part should be already lithified or partially lithified at the time of deposition of the upper hardground part, giving the planar and regular boundary between the two parts (Figure 4). The ^{14}C dating indicates a sedimentary hiatus of nearly 900 years exists between the lower and upper part. In the lower hardground part, the radiocarbon age, 6945–6530 cal yrs BP, is consistent with a Holocene transgression and the onset of the hardground formation in other areas at Abu Dhabi (Strohmenger et al., 2010; Lokier et al., 2015; Paul and Lokier, 2017). Radiocarbon ages of the bottom and top of the upper hardground part, 5840–5425 cal yrs BP and 5871–5475 cal yrs BP, suggest a short time of carbonate accumulation (potentially as brief as ca 30 years). The ^{14}C age in the upper hardground part is in accordance with the later stage of sea-level transgression and/or stillstand following the transgression during the lower hardground part.

Mineralogical variations also support the composite nature of the hardground layer in site 2. In the lower hardground part, aragonite contents gradually increase from the bottom to the top, and high-Mg calcite and protodolomite contents gradually decrease upwards (Figure 4). In contrast, in the upper hardground part, aragonite contents gradually decrease from the bottom to the top, and high-Mg calcite and protodolomite contents gradually increase upwards (Figure 4). This study proposes that the lower hardground part with upward-increasing aragonite contents may correspond to increased water depth with sea-level rise. On the other hand, the upper hardground part with upward-decreasing aragonite contents may reflect decreased water depth with reduction of sea-level rise. This is supported by siliciclastic sediments below the lower hardground part and modern sabkha sediments overlying the upper hardground part. Besides, with the aid of the restriction and evaporative climate, a small sea-level change will cause a considerable change of seawater chemistry (like salinity) and carbonate sediment in terms of bioclast types and carbonate minerals, as in the modern Abu Dhabi coastal area discussed by Pederson et al. (2021). With sea-level change, the hardground samples show a similar mineralogical change as that in Pederson et al. (2021), i.e., lower sea level corresponds to more foraminifera with a high-Mg calcite mineralogy (Figure 8). The correlation between $\delta^{13}C_{carb}$, $\delta^{18}O_{carb}$ and bulk carbonate mineralogy demonstrate mineralogical controls on isotopic composition. Particularly, bulk $\delta^{13}C_{carb}$ data displays a positive correlation ($R^2 = 0.56$) with high-Mg calcite abundance (Figure 9), which indicates that intensified environmental restriction and enhanced evaporation leads to an increase in high-Mg calcite bioclasts (mainly foraminifera), causing the increased $\delta^{13}C_{carb}$. Therefore, the increased $\delta^{13}C_{carb}$ and $\delta^{18}O_{carb}$ in the upper hardground part correspond to enhanced evaporation with reduced water depth (Shinn, 1969; Gröcke et al., 2003).

In conclusion, the hardground layer in site 2 is composite, and its lower and upper parts are controlled by sea-level changes in terms of the formation process and carbonate mineralogy. Notably, the lower hardground part is traceable both landward (e.g., in site 1) and seaward (as reported by Paul and Lokier, 2017). However, the upper hardground part disappears landward in site 1 but is replaced by a hardground layer with a ^{14}C dating of 1920–1608 cal yrs BP in a seaward site (Paul and Lokier, 2017). This landward-to-seaward correlation suggests that hardground formation is more favorable during the earlier stage of sea-level rise when the rate of sea-level rise is relatively high. Consistently, active hardground formation nowadays is also occurring during an initial stage of sea-level transgression (Paul and Lokier, 2017).

5.4 Diachroneity of the hardgrounds

A comparison was made between the two hardground sites (sites 1 & 2) of this study and another two sites (sites 3 & 4) reported by Paul and Lokier (2017) also from the sabkha area (Figure 10A). It should be noted that the ^{14}C dating of the hardground (0–256 cal yrs BP) at site 4 is from the poorly lithified interval that is forming at the modern seafloor (Lokier and Steuber, 2009), therefore representing hardground formation in a much later sea-level transgression than other three sites (Figure 10B). Although there is no ^{14}C age data for the well lithified hardground at site 4, Paul and Lokier (2017) suggest that the upper hardground part at site 3 is

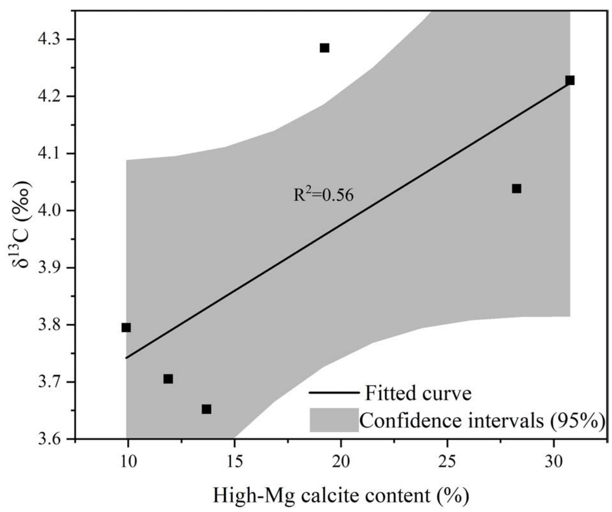

FIGURE 9
The correlation between high-Mg calcite abundance and $\delta^{13}C_{carb}$ values.

related to the well lithified hardground at site 4. Based on the ^{14}C dating, the timing of the lower hardground part in site 2 is well comparable with that in site 1 and site 3. In detail, the ^{14}C age of the most seaward site (site 3) is slightly earlier than that in sites 1 & 2 of this study, which supports the seaward migration of hardground formation with the sea-level rise. However, the age of ^{14}C dating shows an obvious difference in the upper hardground part in site 2 (5871–5452 cal yrs BP) and site 3 (1920–1608 cal yrs BP). As the upper hardground part was formed mainly related to reduced water depth with the later stage of sea-level transgression and/or stillstand to reduced sea-level rise in site 2 and with regression in site 3, if there is a sedimentary hiatus in site 3, this should be also recorded in site 2. More likely, the timing difference in sites 2 & 3 reflects the landward migration of hardground formation associated with water shoaling (Paul and Lokier, 2017). Therefore, there are older ages in site 2 than in site 3. The results herein and that from Paul and Lokier (2017) confirm the diachroneity in hardground formation. Further implications are that the hardground formation during rapid sea-level rise can be less diachronous than that during sea-level stillstand and regression.

5.5 Implications for ancient hardgrounds

The Holocene hardgrounds in the Abu Dhabi area represent those formed in an Aragonite Sea and are characterized by: planar upper surface with no borings nor encrustation, rapid cementation with active carbonate deposition, composite nature, and diachroneity (Figures 11A, B). The features are obviously different from conventional ancient marine hardgrounds presenting: i) irregular upper surfaces with obvious borings and encrustation; ii) long-time duration; iii) a single sediment phase (Immenhauser et al., 2000; Gruszczyński et al., 2002; Taylor and Wilson, 2003; Sattler et al., 2005; Christ et al., 2012; Wright and Cherns, 2016;

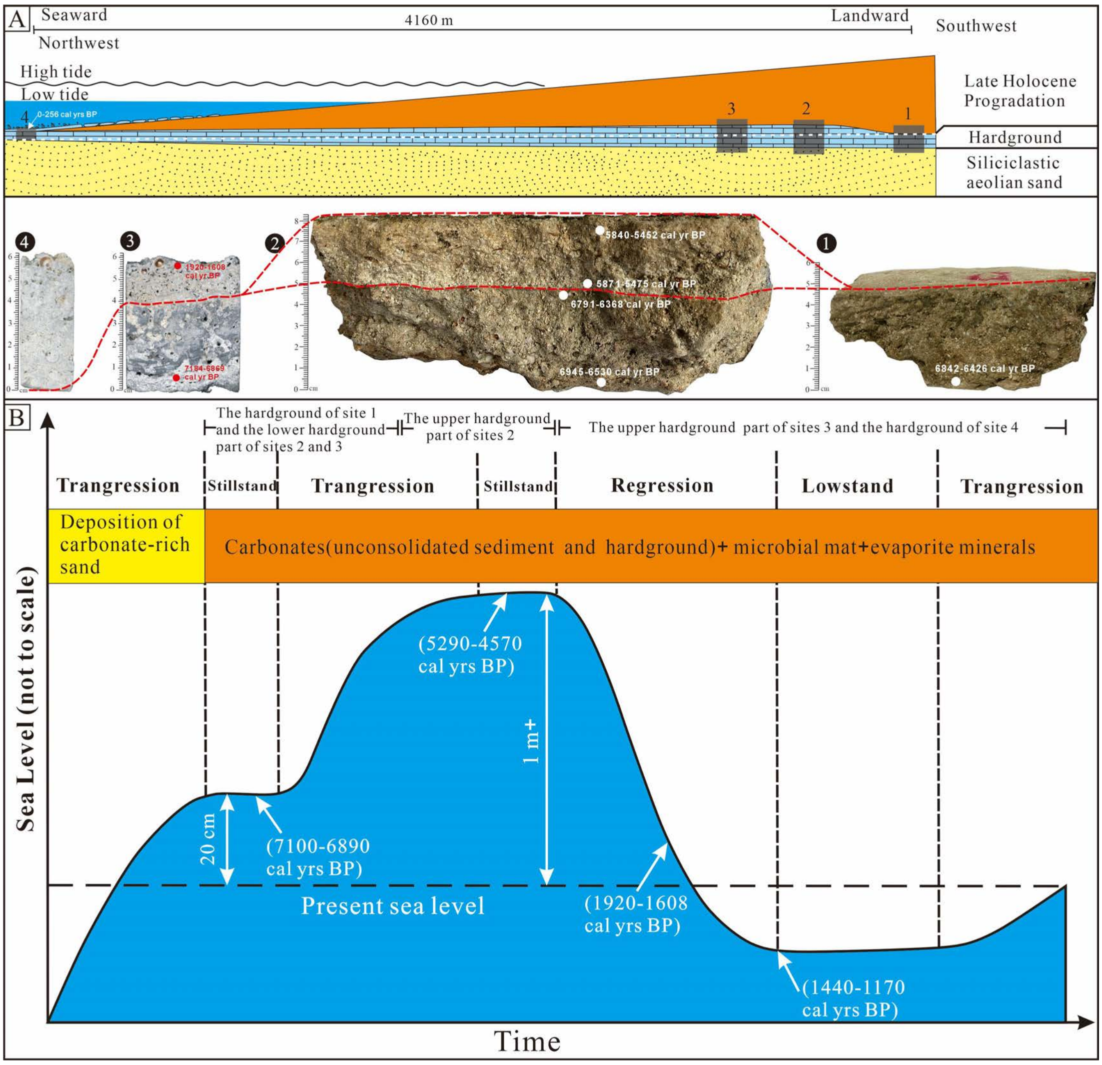

FIGURE 10
The relation between hardground formation and sea-level changes. **(A)** Cross-section of the hardground in Abu Dhabi coastal sabkha (modified after Paul and Lokier, 2017). Sites 1 and 2 are the sampling sites for this study, and sites 3 and 4 are the sampling sites for Paul and Lokier (2017). **(B)** Holocene sea level variations in relation to the formation of the hardgrounds in sites 1-4. The sea-level curve is modified by Paul and Lokier (2017).

Paton et al., 2019; García-Hidalgo and Gil-Gil, 2024) (Figures 11C, D). Given repeat occurrence of Aragonite Seas in the geological past, marine hardgrounds with similar features described in this study may also occur in ancient carbonate records, but difficult to identify. For example, after the Permian-Triassic mass extinction, there was a lack of a large number of hardground-colonizing organisms to settle, and the Triassic hardground was rarely colonized (Bertling, 1999). This may have contributed to the scarcity of reported hardgrounds during this period. In addition, the lack of colonization or erosional exhumation of marine hardgrounds may be related to short seafloor exposure duration (Brett and Brookfield, 1984), high sedimentation rates and rapid cementation. Dissolution, recrystallization, and dolomitization of aragonite or high-Mg calcite can also remove most of the primary hardground evidence (Christ et al., 2015). Due to high aragonite abundance, the marine hardgrounds in this study may experience significant diagenetic alteration (e.g., dissolution, dolomitization), lose their original fabrics, and therefore become difficult to recognize when they are buried. However, with careful microscopic observation, grain fabric preservation favored by early cementation may be detected. Besides, marine hardgrounds are more resistant to erosion from waves, currents, and tidal forces, which can cause different facies changes relative to uncemented carbonate sediments in the stratigraphic records (Paul and Lokier, 2017), which can be used as another diagnostic feature for their recognition. Finally, the multiple stages during hardground formation and lateral diachroneity of the same hardground part cause cautions in using a hardground layer for stratigraphic correlation in science study (e.g., sequence stratigraphy) and application (e.g., oil-gas industry), especially those formed associated with sea-level regression.

6 Conclusion

Marine hardgrounds are common in ancient records but seem to mainly be formed during Calcite Seas. The reasons for this remain unclear and require more hardground information, especially from Aragonite Seas. In this study, a well-developed Holocene marine hardground layer at Abu Dhabi offers new implications for the diagnostic characteristics and formation process of potential "hidden hardgrounds" in the past. Based on new radiocarbon ages and mineralogy variations, the Holocene marine hardground under investigation is considered to form in two stages. The lower hardground part (with a ^{14}C age of 6945–6368 cal yrs BP) corresponding to a transgressive period shows increasing aragonite contents from bottom to top. In contrast, the upper hardground part (with a ^{14}C age of 5871–5452 cal yrs BP)

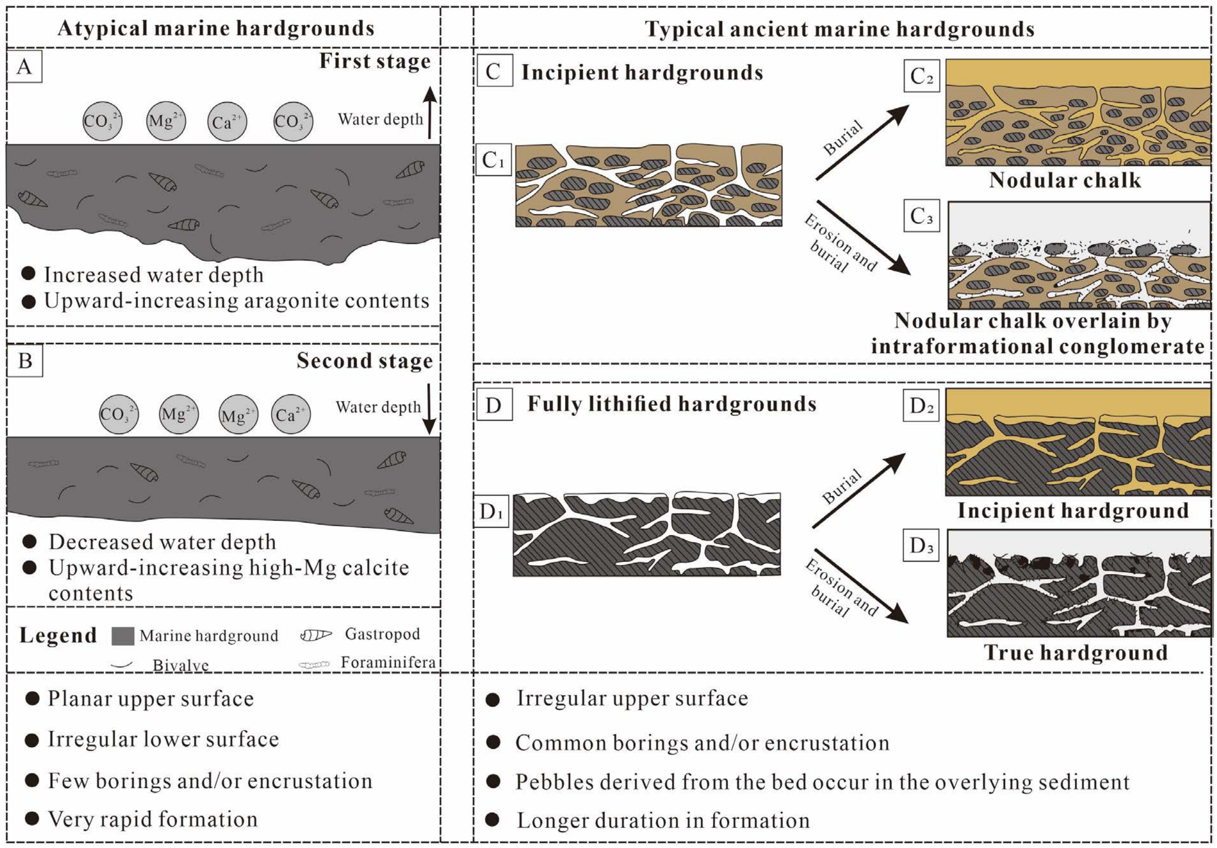

FIGURE 11
Comparison of Characteristics Between Holocene and Ancient Marine Hardgrounds. **(A, B)** Characteristics of atypical Marine Hardgrounds; **(C, D)** Characteristics of Typical Ancient Marine Hardgrounds.

corresponding to the later stage of sea-level transgression and/or stillstand displays increasing high-Mg calcite contents from bottom to top. The marine hardgrounds described in this study are characterized by: planar upper surface with few borings and/or encrustation, rapid cementation with active carbonate deposition, composite nature, and diachroneity, that will be relevant in the identification of similar hardgrounds in ancient sedimentary records (especially in Aragonite Seas). Finally, due to the multiple stages during hardground formation and lateral diachroneity of the same hardground part, caution should be taken in using a hardground layer for stratigraphic correlation.

Data availability statement

The original contributions presented in the study are included in the article/supplementary material. Further inquiries can be directed to the corresponding authors.

Author contributions

CC: Conceptualization, Methodology, Writing – original draft. HZ: Funding acquisition, Supervision, Writing – review & editing. XaW: Investigation, Writing – review & editing. MN: Investigation, Writing – review & editing. XuW: Investigation, Writing – review & editing. HW: Investigation, Writing – review & editing. RT: Data curation, Investigation, Writing – review & editing. MH: Conceptualization, Methodology, Supervision, Writing – review & editing.

Funding

The author(s) declare that financial support was received for the research and/or publication of this article. This study was funded by the National Natural Science Foundation of China (No. 42272131) and Open Foundation of Key Laboratory of Sedimentary Basin and Oil and Gas Resources, Ministry of Natural Resources (No. cdcgs2022003).

Acknowledgments

We are grateful to Kunyang Wang and Guan Wang for their support with the SEM and EDS analyses. Thanks to Dr M. Alsuwaidi for help during field work. We also thank Chenyu Wang for sample treatment. We acknowledge the critical comments of reviewers L. Jovane, J. F. García-Hidalgo, J. Rivers, F. Hasiuk and the editorial guidance of associate editor J. Schijf.

Conflict of interest

RT was employed by PetroChina Southwest Oil & Gasfield Company.

The remaining authors declare that the research was conducted in the absence of any commercial or financial relationships that could be construed as a potential conflict of interest.

Generative AI statement

The author(s) declare that no Generative AI was used in the creation of this manuscript.

Publisher's note

References

Basilone, L., Bernardini, S., Grassa, F., Sulli, A., Nieto, L. M., Abbassi, A., et al. (2024). Paleo-redox conditions during the demise of a carbonate platform in the Tethyan ocean: Evidence from phosphatized and metals (Mn and Fe) rich hardgrounds. *Mar. Pet. Geol.* 170, 107121. doi: 10.1016/j.marpetgeo.2024.107121

Bathurst, R. G. C. (1975). *Carbonate Sediments and Their Diagenesis* (Amsterdam: Elsevier).

Bertling, M. (1999). Taphonomy of trace fossils at omission surfaces (Middle Triassic, East Germany). *Palaeogeogr. Palaeoclimatol. Palaeoecol.* 149, 27–40. doi: 10.1016/S0031-0182(98)00190-4

Brett, C. E., and Brookfield, M. E. (1984). Morphology, faunas and genesis of Ordovician hardgrounds from southern Ontario, Canada. *Palaeogeogr. Palaeoclimatol. Palaeoecol* 46, 233–290. doi: 10.1016/0031-0182(84)90001-4

Brigaud, B., Andrieu, S., Blaise, T., Haurine, F., and Barbarand, J. (2021). Calcite uranium–lead geochronology applied to hardground lithification and sequence boundary dating. *Sedimentology* 68, 168–195. doi: 10.1111/sed.12795

Cander, H. (1995). "Interplay of water-rock interaction efficiency, unconformities, and fluid flow in a carbonate aquifer: Floridan aquifer system," in *Unconformities and Porosity in Carbonate Strata* (Tulsa, Oklahoma, USA: American Association of Petroleum Geologists), vol. 63 . Eds. D. A. Budd, A. H. Saller and P. M. Harris, 103–124. Mem. Am. Ass, petrol. Geol. doi: 10.1306/M63592

Catuneanu, O. (2006). *Principles of Sequence Stratigraphy (Developments in Sedimentology)* (Berlin, Heidelberg: Elsevier).

Catuneanu, O., Abreu, V., Bhattacharya, J. P., Blum, M. D., Dalrymple, R. W., Eriksson, P. G., et al. (2009). Towards the standardization of sequence stratigraphy. *Earth Sci. Rev.* 92, 1–33. doi: 10.1016/j.earscirev.2008.10.003

Christ, N., Immenhauser, A., Amour, F., Mutti, M., Tomas, S., Agar, S. M., et al. (2012). Characterization and interpretation of discontinuity surfaces in a Jurassic ramp setting (High Atlas, Morocco). *Sedimentology* 59, 249–290. doi: 10.1111/j.1365-3091.2011.01251.x

Christ, N., Immenhauser, A., Wood, R., Darwich, K., and Niedermayr, A. (2015). Petrography and environmental controls on the formation of Phanerozoic marine carbonate hardgrounds. *Earth Sci. Rev.* 151, 176–226. doi: 10.1016/j.earscirev.2015.10.002

Clark, P. U., Dyke, A. S., Shakun, J. D., Carlson, A. E., Clark, J., Wohlfarth, B., et al. (2009). The last glacial maximum. *Science* 325, 710–714. doi: 10.1126/science.1172873

Conti, M. A., Girasoli, D. E., Frezza, V., Conte, A. M., Martorelli, E., Matteucci, R., et al. (2013). Repeated events of hardground formation and colonization by endoepilithozoans on the sediment-starved Pontine continental slope (Tyrrhenian Sea, Italy). *Mar. Geol.* 336, 184–197. doi: 10.1016/j.margeo.2012.12.004

Di Stefano, P., and Mindszenty, A. (2000). Fe–Mn-encrusted "Kamenitza" and associated features in the Jurassic of Monte Kumeta (Sicily): subaerial and/or submarine dissolution? *Sediment. Geol.* 132, 37–68. doi: 10.1016/S0037-0738(99)00128

Dravis, J. (1979). Rapid and widespread generation of Recent oolitic hardgrounds on a high energy Bahamian platform, Eleuthera bank, Bahamas. *J. Sediment. Petrol.* 49, 195–207. doi: 10.1306/212F76EE-2B24-11D7-8648000102C1865D

Eren, M. (2022). Marine hardground in the pennsylvanian atoka bank carbonates, eddy county, new Mexico. *Arabian. J. Geosci.* 15, 1646. doi: 10.1007/s12517-022-10932-7

Erhardt, A. M., Turchyn, A. V., Dickson, J. A. D., Sadekov, A. Y., Taylor, P. D., Wilson, M. A., et al. (2020). Chemical composition of carbonate hardground cements as reconstructive tools for Phanerozoic pore fluids. *Geochem. Geophys. Geosyst.* 21, e2019GC008448. doi: 10.1029/2019GC008448

Fleming, K., Johnston, P., Zwartz, D., Yokoyama, Y., Lambeck, K., and Chappell, J. (1998). Refining the eustatic sea-level curve since the Last Glacial Maximum using far- and intermediate-field sites. *Earth Planet. Sci. Lett.* 163, 327–342. doi: 10.1016/S0012-821X(98)00198-8

Friedman, G. M. (1959). Identification of carbonate minerals by staining methods. *J. Sediment. Petrol.* 29, 87–97. doi: 10.1306/74D70894-2B21-11D7-8648000102C1865D

Friedman, G. M. (1998). Rapidity of marine carbonate cementation—implications for carbonate diagenesis and sequence stratigraphy: perspective. *Sediment. Geol.* 119, 1–4. doi: 10.1016/S0037-0738(98)00075-X

García-Hidalgo, J. F., and Gil-Gil, J. (2024). Firmgrounds and hardgrounds in the Coniacian carbonate platform of the Iberian basin: Origin and model for development of omission surfaces in tidal environments. *Sediment. Geol.* 470, 106713. doi: 10.1016/j.sedgeo.2024.106713

Ge, Y. Z., Pederson, C. L., Lokier, S. W., Traas, J. P., Nehrke, G., Neuser, R. D., et al. (2020). Late Holocene to Recent aragonite-cemented transgressive lag deposits in the Abu Dhabi lagoon and intertidal sabkha. *Sedimentology* 67, 2426–2454. doi: 10.1111/sed.12707

Godet, A., Föllmi, K. B., Spangenberg, J. E., Bodin, S., Vermeulen, J., Adatte, T., et al. (2013). Deciphering the message of Early Cretaceous drowning surfaces from the Helvetic Alps: What can be learnt from platform to basin correlations? *Sedimentology* 60, 152–173. doi: 10.1111/sed.12008

Grădinaru, M., Lazăr, I., and Panaiotu, C. E. (2011). Preliminary report on the microfacies analyses of the hardgrounds and condensed horizons associated to the middle Jurassic deposits from Tătarului Gorges (Bucegi Mountains, SE Carpathians). *Acta Palaeontol. Rom.* 7, 169–175.

Grammer, G. M., Crescini, C. M., McNeill, D. F., and Taylor, L. H. (1999). Quantifying rates of syndepositional marine cementation in deeper platform environments–new insight into a fundamental process. *J. Sediment. Res.* 69, 202–207. doi: 10.2110/jsr.69.202

Gröcke, D. R., Price, G. D., Ruffell, A. H., Mutterlose, J., and Baraboshkin, E. (2003). Isotopic evidence for late Jurassic–Early Cretaceous climate change. *Palaeogeogr. Palaeoclimatol. Palaeoecol.* 202, 97–118. doi: 10.1016/S0031-0182(03)00631-X

Gruszczyński, M., Coleman, M. L., Marcinowski, R., Walaszczyk, I., and Isaacs, M. C. (2002). Palaeoenvironmental conditions of hardgrounds formation in the Late Turonian-Coniacian of Mangyshlak Mountains, Western Kazakhstan. *Acta Geol. Pol.* 52, 423–435. doi: 10.1111/j.1467-8624.1964.tb05207.x

Hanebuth, T. J. J., Stattegger, K., and Bojanowski, A. (2009). Termination of the Last Glacial Maximum sea-level lowstand: the Sunda-Shelf data revisited. *Global Planet. Change* 66, 76–84. doi: 10.1016/j.gloplacha.2008.03.011

Heaton, T., Köhler, P., Butzin, M., Bard, E., Reimer, R., Austin, W., et al. (2020). Marine20—The marine radiocarbon age calibration curve (0-55,000 cal BP). *Radiocarbon* 62, 779–820. doi: 10.1017/RDC.2020.68

Hu, Y., Strotz, L. C., Knaust, D., Wang, J., Liang, Y., and Zhang, Z. (2023). Distinguishing borings and burrows in intraclasts: Evidence from the Cambrian (Furongian) of North China. *Sediment. Geol.* 443, 106302. doi: 10.1016/j.sedgeo.2022.106302

Hughen, K. A., Baillie, M. G. L., Bard, E., Beck, J. W., Betrand, C. J. H., Blackwell, P. G., et al. (2004). Marine04 marine radiocarbon age calibration, 0–26 cal kyr BP. *Radiocarbon* 46, 1059–1086. doi: 10.1017/S0033822200033002

Immenhauser, A., Creusen, A., Esteban, M., and Vonhof, H. B. (2000). Recognition and interpretation of polygenic discontinuity surfaces in the middle cretaceous shu'aiba, nahr umr, and natih formations of Northern Oman. *GeoArabia* 5, 299–322. doi: 10.2113/geoarabia0502299

Kennedy, W. J., and Garrison, R. E. (1975). Morphology and genesis of nodular chalks and hardgrounds in the Upper Cretaceous of southern England. *Sedimentology* 22, 311–386. doi: 10.1111/j.1365-3091.1975.tb01637.x

Lee, J. H., Chen, J., and Woo, J. (2015). The earliest Phanerozoic carbonate hardground (Cambrian Stage 5, Series 3): Implications to the paleoseawater chemistry and early adaptation of hardground fauna. *Palaeogeogr. Palaeoclimatol. Palaeoecol.* 440, 172–179. doi: 10.1016/j.palaeo.2015.07.043

Lokier, S. W. (2013). Coastal sabkha preservation in the arabian gulf. *Geoheritage* 5, 11–22. doi: 10.1007/s12371-012-0069-x

Lokier, S. W., Bateman, M. D., Larkin, N. R., Rye, P., and Stewart, J. R. (2015). Late Quaternary sea level changes of the Persian Gulf. *Quat. Res.* 84, 69–81. doi: 10.1016/j.yqres.2015.04.007

Lokier, S. W., and Fiorini, F. (2016). Temporal evolution of a carbonate coastal system, Abu Dhabi, United Arab Emirates. *Mar. Geol.* 381, 102–113. doi: 10.1016/j.margeo.2016.09.001

Lokier, S. W., Knaf, A., and Kimiagar, S. (2013). A quantitative analysis of recent arid coastal sedimentary facies from the Arabian Gulf Coastline of Abu Dhabi, United Arab Emirates. *Mar. Geol.* 346, 141–152. doi: 10.1016/j.margeo.2013.09.006

Lokier, S. W., and Steuber, T. (2008). Quantification of carbonate-ramp sedimentation and progradation rates for the late Holocene Abu Dhabi shoreline. *J. Sediment. Res.* 78, 423–431. doi: 10.2110/jsr.2008.049

Lokier, S. W., and Steuber, T. (2009). Large-scale intertidal polygonal features of the Abu Dhabi coastline. *Sedimentology* 56, 609–621. doi: 10.1111/j.1365-3091.2008.00988.x

Mancini, E. A., Llins, J. C., Parcell, W. C., Aurell, M., Badenas, B., Leinfelder, R. R., et al. (2004). Upper Jurassic thrombolite reservoir play, northeastern Gulf of Mexico. *AAPG. Bull.* 88, 1573–1602. doi: 10.1306/06210404017

Matysik, M., Stachacz, M., Knaust, D., and Whitehouse, M. J. (2022). Geochemistry, ichnology, and sedimentology of omission levels in Middle Triassic (Muschelkalk) platform carbonates of the Germanic Basin (southern Poland). *Palaeogeogr. Palaeoclimatol. Palaeoecol* 585, 110732. doi: 10.1016/j.palaeo.2021.110732

McLaughlin, P. I., Brett, C. E., Wilson, M. A., Pratt, B., and Holmden, C. (2008). Hierarchy of sedimentary discontinuity surfaces and condensed beds from the middle Paleozoic of eastern North America: implications for cratonic sequence stratigraphy. *Geol. Assoc. Can. Spec. Pap.* 48, 175–200.

Millo, C., de Mello, R. M., Leckie, R. M., Benites, M., Giannini, P. C. F., Boggiani, P. C., et al. (2022). Discovery of enigmatic toroidal carbonate concretions on the Rio Grande Rise (Southwestern Atlantic Ocean). *Mar. Geol.* 443, 106665. doi: 10.1016/j.margeo.2021.106665

Moore, C. H. (1989). *Carbonate diagenesis and porosity. Developments in Sedimentology 46* (Amsterdam: Elsevier).

Mutti, M., and Bernoulli, D. (2003). Early marine lithification and hardground development on a miocene ramp (Maiella, Italy): key surfaces to track changes in trophic resources in nontropical carbonate settings. *J. Sediment. Res.* 73, 296–308. doi: 10.1306/083102730296

Palmer, T. J., and Wilson, M. A. (2004). Calcite precipitation and dissolution ofbiogenic aragonite in shallow Ordovician calcite seas. *Lethaia* 37, 417–427. doi: 10.1080/00241160410002135

Pandey, D. K., Fürsich, F. T., Alberti, M., Sharma, J. ,. K., and Swami, N. (2018). Recurrent hardgrounds and their significance for intra-basinal correlations: a case study of upper Bathonian rocks from the western margin of the Indian craton. *J. Palaeogeogr.* 7, 1–12. doi: 10.1186/s42501-018-0013-3

Paton, T. R., Brett, C. E., and Kampouris, G. E. (2019). Genesis, modification, and preservation of complex Upper Ordovician hardgrounds: Implications for sequence stratigraphy and the Great Ordovician Biodiversification Event. *Palaeogeogr. Palaeoclimatol. Palaeoecol.* 526, 53–71. doi: 10.1016/j.palaeo.2019.04.011

Paul, A., and Lokier, S. W. (2017). Holocene marine hardground formation in the Arabian Gulf: Shoreline stabilization, sea level and early diagenesis in the coastal sabkha of Abu Dhabi. *Sediment. Geol.* 352, 1–13. doi: 10.1016/j.sedgeo.2017.02.005

Pederson, C. L., Ge, Y., Lokier, S. W., Swart, P. K., Vonhof, H., Strauss, H., et al. (2021). Seawater chemistry of a modern subtropical 'epeiric'sea: Spatial variability and effects of organic decomposition. *Geochim. Cosmochim. Acta* 314, 159–177. doi: 10.1016/j.gca.2021.09.024

Pigott, J. D., and Land, L. S. (1986). Interstitial water chemistry of Jamaican reefsediment: sulfate reduction and submarine cementation. *Mar. Chem.* 19, 355–378. doi: 10.1016/0304-4203(86)90056-3

Rais, P., Louis-Schmid, B., Bernasconi, S. M., and Weissert, H. (2007). Palaeoceanographic and palaeoclimatic reorganization around the Middle–Late Jurassic transition. *Palaeogeogr. Palaeoclimatol. Palaeoecol.* 251, 527–546. doi: 10.1016/j.palaeo.2007.05.008

Rameil, N., Immenhauser, A., Csoma, A., and Warrlich, G. (2012). Surfaces with a long history: the Aptian top Shu'aiba Formation unconformity, Sultanate of Oman. *Sedimentology* 59, 212–248. doi: 10.1111/j.1365-3091.2011.01279.x

Read, J. F., and Horburry, A. D. (1994). "Eustatic and tectonic controls on porosity evolution beneath sequence-bounding unconformities and parasequence disconformities on carbonate platforms," in *Diagenesis and basin Development*, vol. 36 . Eds. A. D. Horbur and A. G. Robinson (Tulsa Oklahoma USA: AAPG Studies in Geology), 155–197.

Rozhnov, S. V. (2001). "Evolution of the hardground community," in *Ecology of the Cambrian Radiation*. Eds. A. Y. Zhuravlev and R. Riding (Columbia University Press, New York), 238–253.

Sattler, U., Immenhauser, A., Hillgärtner, H., and Esteban, M. (2005). Characterization, lateral variability and lateral extent of discontinuity surfaces on a carbonate platform (Barremian to Lower Aptian, Oman). *Sedimentology* 52, 339–361. doi: 10.1111/j.1365-3091.2005.00701.x

Schlager, W., Reijmer, J. J. G., and Droxler, A. (1994). Highstand shedding of carbonate platforms. *J. Sediment. Res.* 64, 270–281. doi: 10.2110/jsr.69.434

Shinn, E. A. (1969). Submarine lithification of Holocene carbonate sediments in the Persian Gulf. *Sedimentology* 12, 109–144. doi: 10.2113/geoarabia150149

Strohmenger, C. J., Al-Mansoori, A., Al-Jeelani, O., Al-Shamry, A., Al-Hosani, I., Al-Mehsin, K, et al. (2010). The sabkha sequence at Mussafah Channel (Abu Dhabi, United Arab Emirates): facies stacking patterns, microbial-mediated dolomite and evaporite overprint. *GeoArabia*, 15(1), 49–90. doi: 10.2113/geoarabia150149

Taylor, J. C. M., and Illing, L. V. (1969). Holocene intertidal calcium carbonate cementation, Qatar, Persian Gulf. *Sedimentology* 12, 69–107. doi: 10.1111/j.1365-3091.1969.tb00165.x

Taylor, P. D., and Wilson, M. A. (2003). Palaeoecology and evolution of marine hard substrate communities. *Earth Sci. Rev.* 62, 1–103. doi: 10.1016/S0012-8252(02)00131-9

Tucker, M. E., and Wright, V. P. (1990). *Carbonate Sedimentology* (Oxford: Blackwell Scientific Publications), 1–482.

Vinn, O., and Wilson, M. A. (2010). Early large borings from a hardground of Floian-Dapingian age (Early and Middle Ordovician) in northeastern Estonia (Baltica). *Carnets. Géol.* 10, 1–4. doi: 10.4267/2042/35594

Wagner, P. D., Tasker, D. R., and Wahlman, G. P. (1995). "Reservoir degradation and compartmentalization below subaerial exposure unconformities: limestone examples from West Texas, China and Oman," in *Unconformities and Porosity in Carbonate Strata*. Eds. D. A. Budd, A. H. Saller and P. M. Harris (American Association of Petroleum Geologists, Tulsa), 177–195.

Warme, J. E. (1975). "Borings as trace fossils, and the processes of marine bioerosion," in *The Study of Trace Fossils*. Ed. R. W. Frey (Springer, Berlin, Heidelberg), 181–227. doi: 10.1007/978-3-642-65923-2_11

Wignall, P. B. (1993). Distinguishing between oxygen and substrate control in fossil benthic assemblages. *J. Geol. Soc Lond.* 150, 193–196. doi: 10.1144/gsjgs.150.1.0193

Wilson, M. A., and Palmer, T. J. (1992). *Hardgrounds and Hardground Faunas* Vol. 9 (Wales UK: University of Wales, Aberystwyth, Institute of Earth Studies Publications), 1–131.

Wright, V. P., and Cherns, L. (2016). How far did feedback between biodiversity and early diagenesis affect the nature of Early Palaeozoic sea floors? *Palaeontology* 59, 753–765. doi: 10.1111/pala.12258

Yilmaz, I. O., Altiner, D., Tekin, U. K., and Ocakoglu, F. (2012). The first record of the "Mid-Barremian" Oceanic Anoxic Event and the Late Hauterivian platform drowning of the Bilecik platform, Sakarya Zone, western Turkey. *Cretaceous. Res.* 38, 16–39. doi: 10.1016/j.cretres.2012.04.010